Z. Phys. C – Particles and Fields 38, 521–533 (1988)

Zeitschrift für Physik C Particles and Fields


# Measurement and analysis of the reaction $\gamma\gamma \to \pi^+\pi^-\pi^+\pi^-$

PLUTO Collaboration

Ch. Berger, H. Genzel, W. Lackas, J. Pielorz[1]
F. Raupach, W. Wagner[2]
I. Physikalisches Institut der RWTH Aachen[3], D-5100 Aachen, Federal Republic of Germany

A. Klovning, E. Lillestöl
University of Bergen[4], N-5014 Bergen, Norway

J. Bürger, L. Criegee, A. Deuter, F. Ferrarotto[5], G. Franke, M. Gaspero[5], Ch. Gerke, G. Knies, B. Lewendel[6], J. Meyer, U. Michelsen, K.H. Pape, B. Stella[5], U. Timm, G.G. Winter, M. Zachara[7], W. Zimmermann
Deutsches Elektronen-Synchrotron DESY, D-2000 Hamburg, Federal Republic of Germany

P.J. Bussey, S.L. Cartwright[8], J.B. Dainton[9], D. Hendry, B.T. King[9], C. Raine, J.M. Scarr, I.O. Skillicorn, K.M. Smith, J.C. Thomson
University of Glasgow[10], Glasgow G12 8QQ, UK

O. Achterberg, V. Blobel, D. Burkart, K. Diehlmann, M. Feindt, H. Kapitza[11], B. Koppitz, M. Krüger[12], M. Poppe[13], H. Spitzer, R. van Staa
II. Institut für Experimentalphysik der Universität Hamburg[3], D-2000 Hamburg, Federal Republic of Germany

C.Y. Chang, R.G. Glasser, R.G. Kellogg, S.J. Maxfield[9], R.O. Polvado, B. Sechi-Zorn[1], J.A. Skard, A. Skuja, A.J. Tylka[14], G.E. Welch[15], G.T. Zorn
University of Maryland[16], College Park, MD 20742, USA

F. Almeida[17], A. Bäcker, F. Barreiro[18], S. Brandt, K. Derikum[19], C. Grupen, H.J. Meyer, H. Müller, B. Neumann, M. Rost, K. Stupperich, G. Zech
Universität-Gesamthochschule Siegen[3], D-5900 Siegen, Federal Republic of Germany

G. Alexander, G. Bella, Y. Gnat, J. Grunhaus
Tel-Aviv University[20], Ramat Aviv, Tel-Aviv 699 78, Israel

H. Junge, K. Kraski, C. Maxeiner, H. Maxeiner, H. Meyer, D. Schmidt
Universität-Gesamthochschule Wuppertal[3], D-5600 Wuppertal, Federal Republic of Germany

Received 22 December 1987

[1] Deceased
[2] Present address: University of California at Davis, Davis, CA 95616, USA
[3] Supported by the BMFT, FRG
[4] Partially supported by the Norwegian Council for Science and the Humanities.
[5] Rome University, partially supported by I.N.F.N., Sezione di Roma, I-00135 Rome, Italy
[6] Present address: I. Institut für Experimentalphysik der Universität Hamburg, D-2000 Hamburg, FRG
[7] Institute of Nuclear Physics, PL-30059 Cracow, Poland
[8] Present address: SLAC, Stanford, USA
[9] Present address: University of Liverpool, Liverpool, L69 3BX, UK
[10] Supported by the UK. Science and Engineering Research Council
[11] Present address: Carleton University, Ottawa, Ontario, Canada K1S 5B6
[12] Present address: Universität Karlsruhe, D-7500 Karlsruhe, FRG
[13] Present address: CERN-EP, Switzerland
[14] Present address: Cosmic Ray Astrophysics Branch, Code 4154.8, U.S. Naval Research Laboratory, Washington, DC 20375, USA
[15] Present address: Texas Accelerator Center, 2319 Timberland Place, The Woodlands, TX 77380, USA
[16] Partially supported by the Department of Energy, USA
[17] Present address: Instituto di Fisica, Universidad Federal do Rio de Janeiro, Ilha do Fundao, Rio de Janeiro, RJ. Brazil
[18] Present address: Universidad Autonoma de Madrid, Canto Blanco, Madrid 34, Spain
[19] Present address: BESSY, D-1000 Berlin
[20] Partially supported by the Israeli Academy of Sciences and Humanities, Basic Research Foundation

**Abstract.** We have measured the cross section of four charged pion production in photon-photon interactions in the invariant mass range $1.0 \leqq W_{\gamma\gamma} \leqq 3.2$ GeV and up to $Q^2 = 16$ GeV$^2$. For 1.2 GeV $\leqq W_{\gamma\gamma} \leqq 1.7$ GeV the process is dominated by $\rho^0\rho^0$ production with a rapid rise in cross section around 1.2 GeV, well below the nominal $\rho^0\rho^0$ threshold. The observed distributions in the two particle masses and in the production and decay angles are well described by an incoherent sum of the phase-space subprocesses $\gamma\gamma \to \rho^0\rho^0$, $\to \rho^0\pi^+\pi^-$, and $\to \pi^+\pi^-\pi^+\pi^-$. A spin-parity analysis of the $\rho^0\rho^0$ system shows $J^P = 2^+$ to dominate, although $0^+$ is also possible for $W_{\gamma\gamma} \leqq 1.4$ GeV. Negative parity states are excluded.

## 1 Introduction

A large cross section for $\rho^0\rho^0$ production in photon-photon collisions has been observed in several experiments [1–6]. In contrast to $\rho^0\rho^0$ the production of $\rho^+\rho^-$ was shown to be small [7]. There exist a number of attempts to describe these experimental results [8–13] (for reviews see [14–19]). Factorization arguments [8, 9] lead to the interpretation of the broad enhancement in the $\rho^0\rho^0$ cross section around 1.6 GeV as a normal threshold behaviour. Some models suggest an intermediate $\rho^0\rho^0$ resonance [11, 13]. The proposed models differ substantially in the predicted cross sections for pair production of other vector mesons, e.g. $\gamma\gamma \to \rho^0\omega, \gamma\gamma \to \phi\phi$.

In this paper we present results on the four-pion cross section in photon-photon scattering. The data were obtained 1981/82 at PETRA with the detector PLUTO in a dedicated two-photon experiment. The acceptance is good down to small polar angles, due to the installation of two forward spectrometers. A total integrated luminosity of 45 pb$^{-1}$ was collected at an average $e^+e^-$ center of mass energy of 34.7 GeV.

Section 2 gives a brief survey of the detector and the data selection. In Sect. 3 the relative contributions of $\pi^+\pi^-\pi^+\pi^-$(NR)*, $\rho^0\pi^+\pi^-$, and $\rho^0\rho^0$-production are given and the total cross section on $\gamma\gamma \to \pi^+\pi^-\pi^+\pi^-$ for no-tag and single-tag data is evaluated. To check the interpretation of the enhancement as a resonance a spin-parity analysis is performed, and cross sections for different spin-parity assignments are given. Section 4 gives a comparison with other results and a discussion of possible theoretical interpretations. Section 5 gives a final summary.

* So as not to confuse the total cross section for $\gamma\gamma \to \pi^+\pi^-\pi^+\pi^-$ with the non-resonant subprocess $\gamma\gamma \to \pi^+\pi^-\pi^-\pi^-$ we add in brackets NR to the latter

## 2 Detector description and data selection

The data presented here were obtained at the PETRA storage ring at DESY with a beam energy of 17.34 GeV ($\sqrt{s} = 34.7$ GeV) using the PLUTO detector which has been described in detail elsewhere [20]. The central detector consists of 13 cylindrical multiwire proportional chambers (MWPCs) in a 1.65 T magnetic field, which measure charged particles for polar angles $\Theta \geqq 25°$. The momentum resolution is $\sigma_p/p = 5\%$ for momenta relevant to this analysis. The total material seen by a particle traversing the central detector is 0.30 radiation lengths. Photons are detected in the endcap shower counters ($0.58 \leqq |\cos\Theta| \leqq 0.95$; $\sigma_E/E = 19\%/\sqrt{E/\text{GeV}}$) and in the barrel shower counter ($|\cos\Theta| \leqq 0.64$; $\sigma_E/E = 28\%/\sqrt{E/\text{GeV}}$).

In addition, two forward spectrometers [21] measure charged particles between 90 and 260 mrad and photons between 23 and 260 mrad. Charged particles are measured in the forward spectrometers with a momentum resolution of $\sigma_p/p = 3\% \cdot p$[GeV]. Electrons and photons are identified and measured in shower counters. The shower energy resolution is $16.5\%/\sqrt{E/\text{GeV}}$ for the small angle tagger (SAT, 23 mrad $\leq \Theta \leq$ 60 mrad), and $25\%/\sqrt{E/\text{GeV}}$ in the large angle tagger (LAT, 85 mrad $\leqq \Theta \leqq$ 300 mrad).

The angular coverage of the full detector is 93% of $4\pi$ for the tracking chambers, and 99% of $4\pi$ for electromagnetic shower counters. The total integrated luminosity used was 28.7 pb$^{-1}$ for the no-tag and 26.3 pb$^{-1}$ for the single-tag sample.

The essential trigger condition for no-tag events was the track trigger of the central detector. It required at least two tracks extending to MWPC 12 with $|\cos\Theta| \leqq 0.8$ and transverse momenta greater than 350 MeV/c, separated by an azimuthal angle larger than 84°. The experimental trigger for single-tag events required a SAT shower energy of at least 6 GeV in conjunction with at least one track extending to MWPC 6 in the central detector, or a high energy deposit ($\geqq 4$ GeV) in the LAT. The track trigger was fully efficient for tracks at $|\cos\Theta| \leqq 0.8$ with transverse momenta to the $e^+e^-$-beam axis greater than 150 MeV/c. The LAT trigger was efficient (98%) for energies $\geqq 8$ GeV [23].

Photon-photon interactions are characterized by a total invariant mass $W_{\gamma\gamma}$ which can be determined from the two scattered electrons, if both are detected (double-tag events). The majority of data, however, comes from no-tag and single-tag events, for which the invariant mass must be determined from the hadronic final state. For our analysis we used data with $1.0 \leqq W_{\gamma\gamma} \leqq 3.2$ GeV. Most of the data are from the

no-tag sample, where both scattered leptons remain in the beam pipe and are not detected. The average $Q^2$ for these no-tag events is $\langle Q^2 \rangle = 0.008\ \mathrm{GeV}^2$ [22]. In the single-tag case the $Q^2$ coverage is $0.1 \leqq Q^2 \leqq 1\ \mathrm{GeV}^2$ for the small angle tagger (SAT) and $1.0 \leqq Q^2 \leqq 16\ \mathrm{GeV}^2$ for the large angle tagger (LAT).

The data for the reaction $\gamma\gamma \to \pi^+\pi^-\pi^+\pi^-$ were selected from the triggered events by requiring events with four charge balanced tracks and no additional photons (no shower energy cluster with more than 100 MeV). The tracks had to be fully reconstructed (at least five points in the $r-\varphi$ plane), and had to originate from the interaction point within a transverse distance of less than 2.0 cm (rsp. 4.0 cm) for particles in the central detector (rsp. in the forward spectrometers). A longitudinal distance cut of $\leqq 4.0$ cm with respect to the interaction point was applied. At least three of the four tracks had to have a momentum of $\geqq 150$ MeV/c. The squared sum of transverse momenta $|\Sigma\, \mathbf{p}_T|^2$ was used to select exclusive $\gamma\gamma$-events. For the no-tag sample and for the single-tag sample (where the transverse momentum of the tagged electron was included) we demanded $|\Sigma\, \mathbf{p}_T|^2 \leqq 0.10\ \mathrm{GeV}^2$ and $|\Sigma\, \mathbf{p}_T|^2 \leqq 0.15\ \mathrm{GeV}^2$, respectively. These selections yielded 198 single-tag and 2272 no-tag events with $1.0 \leqq W_{\gamma\gamma} \leqq 3.2$ GeV.

The background from cosmic rays, beam-gas interactions and off-momentum particles was estimated from the side bands in the longitudinal vertex distribution of fitted tracks to be 1.2% for no-tag and 0.9% for single-tag events. The background from other processes was determined from Monte Carlo studies to be 1.0 event from the channel $e^+e^- \to$ hadrons, 0.7 events from the channel $e^+e^- \to \tau^+\tau^-$, and 2.0 events from the reaction $\gamma\gamma \to \tau^+\tau^-$ in the no-tag sample. For the single-tag sample the total background was less than one event. Since the number of background events was low, we did not subtract the background, but included it in the systematic error.

PLUTO has a limited ability to identify hadrons. Therefore, the four-track sample contains also events such as $\gamma\gamma \to K^+K^-\pi^+\pi^-$. The cross section for this process in the kinematic range considered here is, however, small [5, 24].

## 3 Determination of the total cross section for $\gamma\gamma \to \pi^+\pi^-\pi^+\pi^-$

### 3.1 Pion pair spectra

For a final state of four charged pions, four unlike-sign two pion combinations and two like-sign combinations can be constructed. Figure 1a, b shows the mass distributions for the unlike-sign combinations in the no-tag and single-tag data, with four entries per event. Also given are the distributions of the corresponding like-sign combinations (two entries per event, hatched histograms).

The mass distributions of the unlike-sign combinations exhibit a clear $\rho^0$-signal. This is improved by subtracting the combinatorial background given by the mass distribution of the like-sign combinations (Fig. 1c, d). A fit to the data gives a $\rho^0$ mass and width in good agreement with the known $\rho^0$ parameters [25]. These mass plots and in particular the scatter plots of the $\pi\pi$ mass combinations (Fig. 2a, b) indicate that a large fraction of the four pion final state originates from an intermediate $\rho^0\rho^0$ state. These scatter plots represents the input data for the

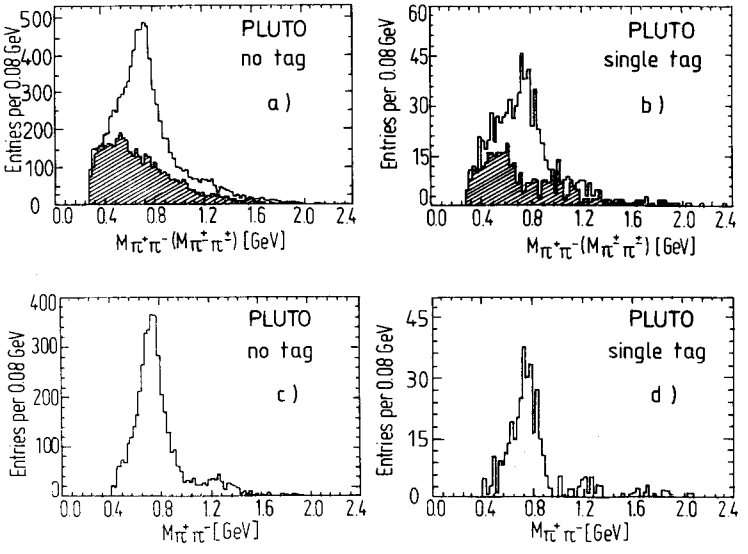


**Fig. 1. a, b** Mass distributions for two-pion like-sign (shaded area) and unlike-sign combinations for no-tag and single-tag data. **c, d** Corrected two pion unlike-sign mass distributions for no-tag and single-tag data

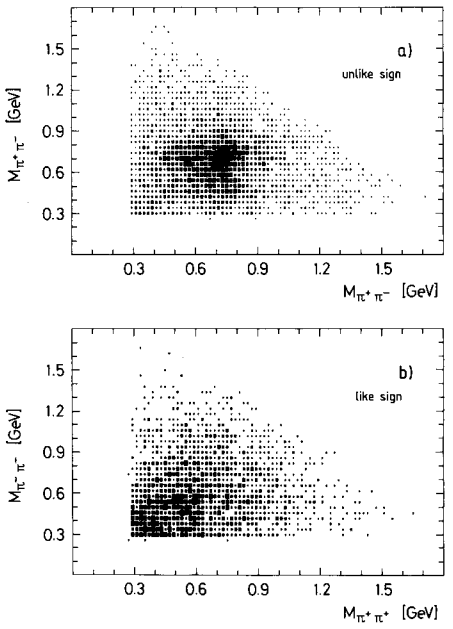


**Fig. 2a, b.** Scatter plots of $\pi\pi$ mass combinations for unlike- and like-sign pions

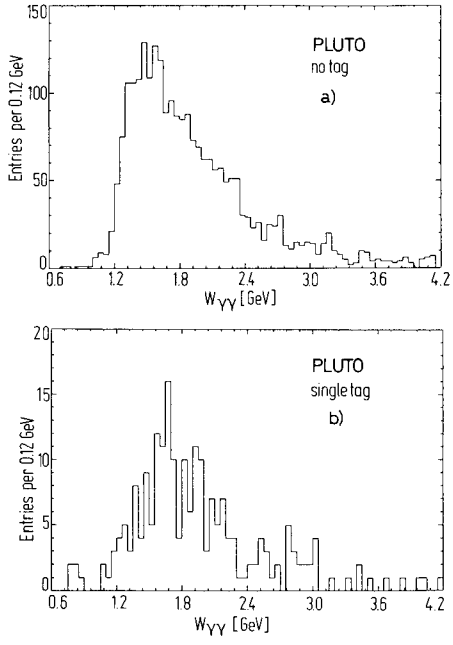


**Fig. 3a, b.** Invariant mass distribution of four pion final states for no-tag **a** and single-tag **b** data

decomposition of the toal cross section into various subprocesses (see Sect. 3.3 and 3.4).

The invariant mass distribution of the four pion final states is shown in Fig 3a, b for the no-tag and single-tag case. It exhibits a steep rise around $W_{\gamma\gamma} \approx 1.2$ GeV well below the nominal $\rho^0\rho^0$ threshold and falls slowly towards large $W_{\gamma\gamma}$ values. The maximum is reached around $W_{\gamma\gamma} \approx 1.6$ GeV.

### *3.2 Monte Carlo models and acceptances*

To obtain quantitative estimates of the number of $\rho^0$-mesons in the four pion data sample, we have converted the invariant $W_{\gamma\gamma}$ distributions to $\pi^+\pi^-\pi^+\pi^-$ cross sections by adopting three models for the production of a four pion final state, namely

$\gamma\gamma \to \pi^+\pi^-\pi^+\pi^-$ (phase space, non-resonant (NR))
$\gamma\gamma \to \rho^0\pi^+\pi^-$ $\to \pi^+\pi^-\pi^+\pi^-$ (isotropic)
$\gamma\gamma \to \rho^0\rho^0$ $\to \pi^+\pi^-\pi^+\pi^-$ (isotropic)

The conversion of the $W_{\gamma\gamma}$-mass distributions into cross sections is model dependent, because the detector acceptance depends on the production model. The detector acceptance was calculated using Monte Carlo generated events and passing them through the detector simulation and analysis programs. All cuts are identical for real data and Monte Carlo events.

The above three models for the production of a four pion final state were considered, and in addition five possible models for the production and decay of a hypothetial resonance $R$ with fixed spin and parity decaying into four pions via $\rho^0\rho^0$. The allowed spin-parity assignments for $R$ are

$$J^P = 0^+, 0^-, 2^+(0), 2^+(2), 2^-$$

where for $2^+$ two different helicity states are taken into account. Interferences between the various helicity states are neglected, and only the lowest possible angular momenta are taken into account. In the following, the Monte Carlo implementation of the theoretical models is briefly described.

Firstly, the momenta of the scattered leptons were generated. This was done by adapting the program of Kawabata [26] which uses the exact formalism of Budnev et al. [27] for the differential cross section [28]. Secondly, a phase space decay of the invariant mass $W_{\gamma\gamma}$ into two positive and two negative pions was performed. Data sets for the different models were then obtained by weighting the events with squared matrix elements [2, 6]. At fixed $W_{\gamma\gamma}$ the differential cross section depends on a set of seven variables, which can symbolically be written as

$$\xi = (m_{12}^2, m_{34}^2, \vartheta_\rho^{12}, \vartheta_\pi^{12}, \varphi_\pi^{12}, \vartheta_\pi^{34}, \varphi_\pi^{34}).$$

Here $m_{ij}$ denotes the invariant mass of pions $i$ and $j$. $\vartheta_\rho^{ij}$ is the angle of this system with respect to the $\gamma\gamma$-axis in the $\gamma\gamma$ center of mass system. $\vartheta_\pi^{ij}$ and $\varphi_\pi^{ij}$ are the polar and azimuthal angles of the positive

pion $i$ in the center of mass of the system $ij$ with the $z$-axis parallel to the $\gamma\gamma$-axis (see Fig. 8).

In order to determine the $\rho^0$ content in the four pion sample, we have used the models for $\rho^0\rho^0$ and $\rho^0\pi^+\pi^-$ introduced by the TASSO Collaboration [2] in which the differential production cross section is represented as:

$$\frac{d^7\sigma_i}{d\xi^7} = C(W_{\gamma\gamma}) \cdot R_4(W_{\gamma\gamma}, \xi) \cdot |g_i(\xi) \cdot g_i'(W_{\gamma\gamma})|^2.$$

Here $R_4(W_{\gamma\gamma}, \xi)$ is the four particle phase space density; $g_i'(W_{\gamma\gamma})$ and $g_i(\xi)$ represent the $W_{\gamma\gamma}$- and $\xi$-dependent parts of the particular production mechanism $i$. The flux factors are absorbed in $C(W_{\gamma\gamma})$. $g_i(\xi)$ describes the resonance production in the $\pi^+\pi^-$-channel and can contain angular correlations. $g_i'(W_{\gamma\gamma})$ describes the $W_{\gamma\gamma}$ dependence of the matrix element, which in our analysis is taken to be constant with respect to $W_{\gamma\gamma}$.

The four pion phase space density $R_4(W_{\gamma\gamma}, \xi)$ is the same for all subprocesses. The matrix element $g_i(\xi)$ discriminates between the subprocesses, where $i = \rho^0\rho^0, \rho^0\pi^+\pi^-$ and $\pi^+\pi^-\pi^+\pi^-$(NR). Only isotropic production and decay of the final states are considered in the first model. Thus $g_i(\xi)$ does not depend on the angular coordinates.

Since pions are bosons, $g_i(\xi)$ must be symmetric under interchange of two pions with the same charge. The appropriate functions satisfying these requirements are:

$$\begin{aligned} g_{\pi^+\pi^-\pi^+\pi^-} &= 1, \\ g_{\rho^0\pi^+\pi^-} &= \tfrac{1}{2}\{\mathrm{BW}(m_{12}) + \mathrm{BW}(m_{34}) \\ &\quad + \mathrm{BW}(m_{14}) + \mathrm{BW}(m_{23})\}, \\ g_{\rho^0\rho^0} &= \frac{1}{\sqrt{2}}\{\mathrm{BW}(m_{12}) \cdot \mathrm{BW}(m_{34}) \\ &\quad + \mathrm{BW}(m_{14}) \cdot \mathrm{BW}(m_{23})\} \end{aligned}$$

where $\mathrm{BW}(m_{ij})$ are relativistic Breit-Wigner amplitudes for the unlike-sign combination of the pion $i$ with the pion $j$ [29]. It is important to note that this weighting procedure introduces no angular correlations. The decay of the object of invariant mass $W_{\gamma\gamma}$ is still isotropic for these three subprocesses.

If it is assumed that an intermediate state $R$ with given quantum numbers is formed and decays into four pions via $\rho^0\rho^0$, the four pion phase space is weighted by covariant spin-parity amplitudes, which have been calculated by Poppe [14]. The weights involve in this case not only the relativistic Breit-Wigner amplitudes of the possible $\pi^+\pi^-$ combinations, but also the momentum vectors of the pions and angles describing the relative orientation of these vectors in space. The latter introduces angular dependences.

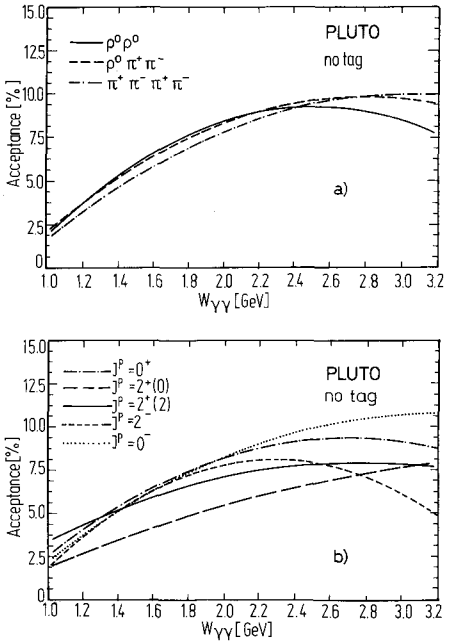


**Fig. 4a, b.** Detector acceptance for the phase space like subprocesses $\gamma\gamma \to \rho^0\rho^0, \to \rho^0\pi^+\pi^-, \to \pi^+\pi^-\pi^+\pi^-$ (NR) **a**, and for five different spin-parity states $J^P$ decaying to $\rho^0\rho^0$ **b**

The acceptance is then calculated in the usual fashion by passing the Monte Carlo generated events through the PLUTO detector simulation and the chain of selection and analysis programs. The acceptance is the ratio between accepted and generated events and depends on the model, the invariant mass $W_{\gamma\gamma}$ and the $Q^2$ of the virtual photon. The absorption of pions in the beam pipe and the detector material leads to an event loss of 21% [31]. Figure 4a, b shows the acceptances for the three subprocesses used and also for the five spin-parity assignments of $R$ . In the relevant kinematic range of $W_{\gamma\gamma}$ the acceptances vary typically between 3% at 1.2 GeV and 8% at 3.0 GeV; 28% of the acceptance is due to the two forward spectrometers.

### *3.3 Decomposition into partial cross sections*

We now do a 3-parameter fit to determine the relative fractions of the subprocesses $\gamma\gamma \to \rho^0\rho^0$, $\gamma\gamma \to \rho^0\pi^+\pi^-$, and $\gamma\gamma \to \pi^+\pi^-\pi^+\pi^-$(NR). For the fitting procedure, a maximum likelihood method for Poisson distributed data was used as follows.

For fixed bins in $W_{\gamma\gamma}$ (or in $Q^2$), typically 100 MeV (rsp. 0.3 GeV$^2$) wide, we construct two-dimensional scatter diagrams, in which each $\pi^+\pi^-(\pi^\pm\pi^\pm)$ mass combination is plotted against the other mass combination. These are fitted by a linear combination of the three subprocesses. The likelihood function is de-

fined by

$$\mathcal{L} = \prod_{i=1}^{N} P(N_{\exp}(i), F(i))$$

where the product runs over the $N$ events in the $W_{\gamma\gamma}$ (or $Q^2$) bin. The probability of observing $N_{\exp}(i)$ events for the expected value $F(i) = F(\lambda, N_{MC}(i))$ is given by

$$P(N_{\exp}(i), F(i)) = F(i)^{N_{\exp}(i)} \cdot \frac{e^{-F(i)}}{N_{\exp}(i)!}$$

and the expectation value of the hypothesis can be written as

$$F(i) = \sum_{j=1}^{n} \lambda_j N_j^{MC}(i)$$

with the constraint $\sum_{j=1}^{n} \lambda_j = 1$.

$N_{\exp}(i)$ are the experimental numbers of combinations in typically 50 MeV by 50 MeV wide mass squared bins in the scatter plot, $N_j^{MC}(i)$ is the same quantity for the Monte Carlo model $j$. The $\lambda_j$ are the fractions of the models which are varied in the fit to maximize $\mathcal{L}$. The sum runs over the $n$ contributions considered in a given fit (up to seven). For each model assumption the total number of Monte Carlo generated events $\sum_{i=1}^{N} N^{MC}(i)$ is normalized to the number of measured events. To check the fitting procedure, we generated samples of events according to different models and tried to recover them by the fit. The input data could be reproduced almost exactly thus demonstrating the reliability of the procedure. The fit to the invariant mass distributions is performed in various $W_{\gamma\gamma}$ and $Q^2$ ranges. A similar procedure was employed to determine the contributions from the different spin-parity states to the process $\gamma\gamma \to R \to \rho^0\rho^0$ (see Sect. 3.4).

The result of the 3-parameter fit to the no-tag data is given in Table 1a. The subprocess $\gamma\gamma \to \rho^0\rho^0$ dominates in the $W_{\gamma\gamma}$ range between 1.2 GeV and 1.7 GeV. The contribution from $\gamma\gamma \to \rho^0\pi^+\pi^-$ in this energy range is compatible with zero. The procedure was therefore repeated with a 2-parameter fit, yielding the contributions listed in Table 1b. Also given are the $\chi^2$ per degree of freedom and the number of degrees of freedom.

The fractions of $\gamma\gamma \to \rho^0\rho^0$ and $\gamma\gamma \to \pi^+\pi^-\pi^+\pi^-$ (NR) as derived from fits with and also without the $\rho^0\pi^+\pi^-$ term are shown in Fig. 5a, b. When comparing them with those of TASSO, CELLO, and TPC/2$\gamma$ (Fig. 5a, b) one has to keep in mind that there may be systematic differences due to different models used for acceptance corrections.

**Table 1a.** Fractions [%] of the subprocesses $\gamma\gamma \to \rho^0\rho^0$, $\to \rho^0\pi^+\pi^-$, and $\to \pi^+\pi^-\pi^+\pi^-$ (NR) as derived from a 3-parameter fit to the no-tag data

| $W_{\gamma\gamma}$(GeV) | $\rho^0\rho^0$ | $\rho^0\pi^+\pi^-$ | $\pi^+\pi^-\pi^+\pi^-$ | $\chi^2$/NDF | NDF |
|---|---|---|---|---|---|
| 1.0–1.2 | 28±8 | 49±17 | 23±15 | 1.7 | 32 |
| 1.2–1.3 | 68±7 | 20±11 | 12± 7 | 1.7 | 42 |
| 1.3–1.4 | 80±5 | 5± 8 | 15± 5 | 1.6 | 65 |
| 1.4–1.5 | 85±5 | −1± 7 | 16± 4 | 1.3 | 89 |
| 1.5–1.6 | 67±4 | 10± 7 | 22± 5 | 1.5 | 107 |
| 1.6–1.7 | 73±6 | 10± 8 | 17± 5 | 1.2 | 102 |
| 1.7–1.8 | 59±7 | 18± 9 | 23± 5 | 1.6 | 101 |
| 1.8–1.9 | 40±7 | 27± 8 | 33± 5 | 1.2 | 104 |
| 1.9–2.0 | 20±7 | 53± 9 | 27± 6 | 1.9 | 91 |
| 2.0–2.1 | 17±6 | 42± 9 | 41± 6 | 0.9 | 83 |
| 2.1–2.2 | 29±7 | 30± 9 | 41± 7 | 1.5 | 68 |
| 2.2–2.3 | 18±5 | 29± 9 | 53± 7 | 0.8 | 61 |
| 2.3–2.4 | 18±7 | 27±11 | 55± 8 | 1.3 | 44 |
| 2.4–2.6 | 17±6 | 47± 9 | 36± 7 | 1.2 | 63 |
| 2.6–2.8 | 14±6 | 55± 9 | 31± 7 | 1.4 | 59 |
| 2.8–3.0 | 18±7 | 43±11 | 39± 8 | 1.2 | 28 |
| 3.0–3.2 | 25±7 | 37±12 | 38±10 | 1.2 | 26 |

**Table 1b.** Fractions [%] of the subprocesses $\gamma\gamma \to \rho^0\rho^0$, and $\to \pi^+\pi^-\pi^+\pi^-$ (NR) as derived from a 2 parameter fit to the no-tag data in the energy range $1.2 \leqq W_{\gamma\gamma} \leqq 1.8$ GeV. The contribution from $\gamma\gamma \to \rho^0\pi^+\pi^-$ is set to zero in this range of $W_{\gamma\gamma}$

| $W_{\gamma\gamma}$(GeV) | $\rho^0\rho^0$ | $\pi^+\pi^-\pi^+\pi^-$ | $\chi^2$/NDF | NDF |
|---|---|---|---|---|
| 1.2–1.3 | 76±6 | 24±6 | 1.7 | 43 |
| 1.3–1.4 | 81±4 | 19±4 | 1.6 | 66 |
| 1.4–1.5 | 85±4 | 15±4 | 1.3 | 90 |
| 1.5–1.6 | 70±4 | 30±4 | 1.4 | 108 |
| 1.6–1.7 | 79±4 | 21±4 | 1.2 | 103 |
| 1.7–1.8 | 70±5 | 30±5 | 1.5 | 102 |

The results of a similar fit to the single-tag data are given in Tables 2a, b. In addition, a 3-parameter fit for various $Q^2$ ranges was carried out (Table 2c). $\rho^0\rho^0$ production dominates at low $Q^2$, decreasing at higher $Q^2$.

The total cross sections of the process $\gamma\gamma \to \pi^+\pi^-\pi^+\pi^-$ and of the subprocess $\gamma\gamma \to \rho^0\rho^0$, as derived from the 3-parameter fit are presented in Fig. 6a, b for the no-tag and single-tag data as a function of the invariant mass of the four pion system. The cross section data are listed in Tables 3 and 4a, b. Only statistical errors are shown.

The $Q^2$ dependence of the single-tag cross sections for $\gamma\gamma \to \rho^0\rho^0$ (Fig. 7) shows a steep fall off towards high $Q^2$. A simple $\rho$-pole (VDM) and also the parameter free predictions of the factorization model of Alexander et al. [8, 9] account well for the data, while an attempt to apply the generalized vector meson dominance model (GVDM) [30] to this reaction fails to do so.

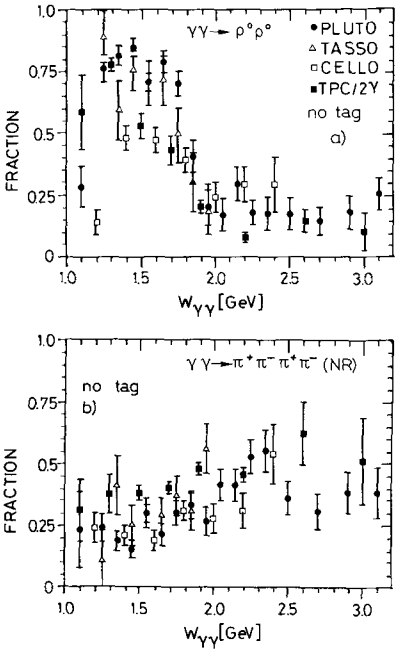


**Fig. 5a, b.** Fractions of the processes $\gamma\gamma \to \rho^0\rho^0$ **a** and $\gamma\gamma \to \pi^+\pi^-\pi^+\pi^-$ (NR) **b** as a function of $W_{\gamma\gamma}$ for the no-tag data. Also shown are the results from TASSO, CELLO, and TPC/2$\gamma$

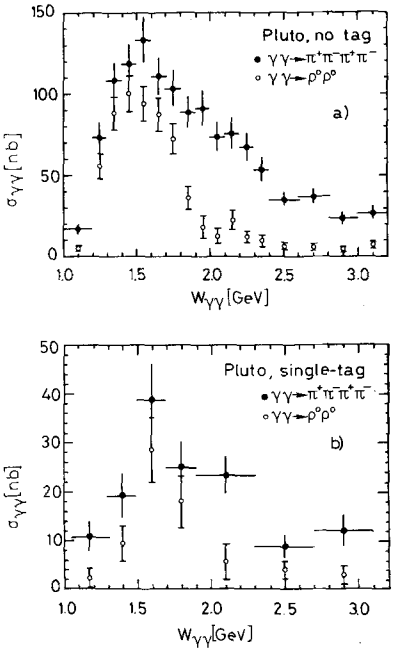


**Fig. 6a, b.** Total cross section of the process $\gamma\gamma \to \pi^+\pi^-\pi^+\pi^-$ (full symbols) and of the subprocess $\gamma\gamma \to \rho^0\rho^0$ with isotropic production and decay of the $\rho^0$'s (open circles) for no-tag **a** and single-tag data **b**

The measured angular distributions can also be compared to the results of the 3-parameter fit. The variables are defined in Fig. 8. $\vartheta_\rho$ is the production angle of one $\rho^0$ in the $\gamma\gamma$ center of mass system. $\vartheta_\pi$ is the polar angle of the decay $\pi^+$ in the rest system of the $\rho^0$('$\rho^0$-helicity system') with respect to the negative direction of flight of the second $\rho^0$. Correspondingly, $\vartheta_{ab}$ is the opening angle between two decay $\pi^+$-directions each defined in its respective $\rho^0$ CM frame. Finally, $\Delta\varphi$ is the azimuthal angle difference between the decay planes of the two $\rho^0$'s.

The measured distribution of the above defined angles is shown in Fig. 9 along with the results of the 2-parameter fits. The data are reproduced well by the sum of $\rho^0\rho^0$ and $\pi^+\pi^-\pi^+\pi^-$ (NR) final states.

### *3.4 Decomposition of the $\rho^0\rho^0$ subchannel into spin-parity states*

The spin-parity analysis is applied only to the no-tag data. We address the question of whether the large cross section for the process $\gamma\gamma \to \rho^0\rho^0$ can be understood as due to the formation of an intermediate resonance with unique quantum numbers. It is the aim of this analysis to find out whether such quantum numbers can be determined, and whether the hypothesis describes the measured angular distributions as well as the incoherent sum of the three (weighted) phase space models.

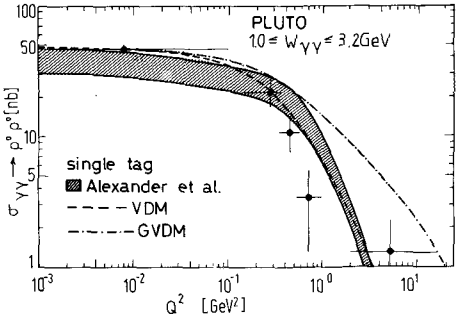


**Fig. 7.** $Q^2$ dependence of the single-tag cross section for the process $\gamma\gamma \to \rho^0\rho^0$. The dashed and dashed-dotted lines are predictions from the VDM and GVDM-models. The prediction based on the factorization models is indicated as hatched band

The five possible spin-parity states of the $\rho^0\rho^0$ system are $J^P = 0^-, 0^+, 2^-, 2^+(0)$, and $2^+(2)$. In this analysis contributions from $\gamma\gamma \to \rho^0\pi^+\pi^-$ and $\gamma\gamma \to \pi^+\pi^-\pi^+\pi^-$ are also allowed, so that seven parameters ($\lambda_{\rho^0\pi^+\pi^-}$; $\lambda_{\pi^+\pi^-\pi^+\pi^-(\mathrm{NR})}$; $\lambda_{\rho^0\rho^0}$ for five $J^P$ states) are fitted. The maximum likelihood analysis was performed as described in Sect. 3 with the inclusion of the angular distributions in the fit procedure. The fractions of the $J^P$-amplitudes resulting from a 7-parameter fit are given in Table 5 for different $W_{\gamma\gamma}$ bins. The corresponding cross sections are listed in Table 6. Also shown are the results for $\gamma\gamma \to \rho^0\rho^0$ from the 3-parameter fit ($\rho^0\rho^0$; $\rho^0\pi^+\pi^-$; $\pi^+\pi^-\pi^+\pi^-$ (NR))

as described in Sect. 3.2. A comparison of these two data sets (Fig. 10a, b) gives an idea of the systematic uncertainties due to the model dependence of the $\rho^0\rho^0$ cross section. In the $W_{\gamma\gamma}$-range where the cross section reaches its maximum, the fit strongly favours the $2^+$ hypothesis. This is also borne out by the angular distributions obtained for the different $J^P$-assignments as shown in Fig. 11a. Negative parity states are ruled out, especially on the basis of the $\Delta\varphi$ and $\cos\vartheta_{ab}$ angular distributions. The $J^P$ states $0^+$ and $2^+(0)$ give a poor fit in the $\Delta\varphi$ distribution, compared to $2^+(2)$. They are acceptable, however, in the other angular variables, although the angles $\vartheta_\rho$ and $\vartheta_\pi$ can hardly discriminate between the different $J^P$-amplitudes. It cannot be excluded that for $W_{\gamma\gamma} \leqq 1.4$ GeV there is some contribution from the $0^+$ state. The 7-parameter fit to the angular distributions is shown in Fig. 11b.

We have also determined the detector acceptance assuming that the $\rho^0\rho^0$-production proceeds entirely through the $J^P=2^+$ state. The resulting cross section for $\gamma\gamma\to\rho^0\rho^0$ (as derived from fitting four parameters ($\pi^+\pi^-\pi^+\pi^-$ (NR); $\rho^0\pi^+\pi^-$; $\rho^0\rho^0\equiv 2^+(2)$, $2^+(0)$), is shown in Fig. 10c. It exhibits a flat enhancement, $\approx 600$ MeV wide.

For further details concerning the analysis and the reliability of the fit procedure the reader is referred to [31].

**Table 2a.** Fractions [%] of the subprocess $\gamma\gamma\to\rho^0\rho^0$, $\to\rho^0\pi^+\pi^-$, and $\pi^+\pi^-\pi^+\pi^-$ (NR) as derived from a 3-parameter fit to the single tag data

| $W_{\gamma\gamma}$(GeV) | $\rho^0\rho^0$ | $\rho^0\pi^+\pi^-$ | $\pi^+\pi^-\pi^+\pi^-$ | $\chi^2$/NDF | NDF |
|---|---|---|---|---|---|
| 1.0–1.3 | 18±22 | 16±46 | 66±41 | 1.9 | 4 |
| 1.3–1.5 | 37±18 | 29±28 | 34±21 | 1.5 | 9 |
| 1.5–1.7 | 72±14 | 3±20 | 25±14 | 1.4 | 18 |
| 1.7–1.9 | 57±21 | 21±26 | 22±16 | 1.5 | 13 |
| 1.9–2.3 | 24±15 | 60±19 | 16±12 | 1.2 | 24 |
| 2.3–2.7 | 46±16 | −10±25 | 64±18 | 2.5 | 4 |
| 2.7–3.1 | 24±14 | 14±25 | 62±21 | 1.7 | 5 |

**Table 2b.** Fractions [%] of the subprocesses $\gamma\gamma\to\rho^0\rho^0$ and $\to\pi^+\pi^-\pi^+\pi^-$ (NR) from a two parameter fit to the single-tag data in the restricted range $1.0\leqq W_{\gamma\gamma}\leqq 1.9$ GeV

| $W_{\gamma\gamma}$(GeV) | $\rho^0\rho^0$ | $\pi^+\pi^-\pi^+\pi^-$ | $\chi^2$/NDF | NDF |
|---|---|---|---|---|
| 1.0–1.3 | 22±17 | 78±17 | 1.6 | 5 |
| 1.3–1.5 | 49±15 | 51±15 | 1.4 | 10 |
| 1.5–1.7 | 74±11 | 26±11 | 1.4 | 19 |
| 1.7–1.9 | 72±15 | 28±15 | 1.3 | 14 |

**Table 3.** Cross sections for the process $\gamma\gamma\to\pi^+\pi^-\pi^+\pi^-$ and the subprocess $\gamma\gamma\to\rho^0\rho^0$ from no-tag data as derived from a 2 parameter fit in the range $1.2\leqq W_{\gamma\gamma}\leqq 1.8$ GeV and a 3-parameter fit for $W_{\gamma\gamma}\leqq 1.2$ GeV and $W_{\gamma\gamma}\geqq 1.8$ GeV

| $W_{\gamma\gamma}$[GeV] | $\sigma_{\pi^+\pi^-\pi^+\pi^-}$ [nb] (phase space acceptance corrected) | $\sigma_{\rho^0\rho^0}$ [nb] |
|---|---|---|
| 1.0–1.2 | 17± 3 | 5± 2 |
| 1.2–1.3 | 73± 9 | 55± 8 |
| 1.3–1.4 | 108±11 | 88±10 |
| 1.4–1.5 | 118±12 | 100±11 |
| 1.5–1.6 | 133±14 | 94±11 |
| 1.6–1.7 | 111±12 | 87±10 |
| 1.7–1.8 | 103±11 | 72± 9 |
| 1.8–1.9 | 88±10 | 36± 7 |
| 1.9–2.0 | 91±11 | 18± 7 |
| 2.0–2.1 | 73± 9 | 12± 5 |
| 2.1–2.2 | 75±10 | 22± 6 |
| 2.2–2.3 | 67± 9 | 12± 4 |
| 2.3–2.4 | 53± 7 | 9± 4 |
| 2.4–2.6 | 35± 4 | 6± 2 |
| 2.6–2.8 | 36± 5 | 5± 2 |
| 2.8–3.0 | 23± 4 | 4± 2 |
| 3.0–3.2 | 26± 4 | 7± 2 |

**Table 2c.** Fractions [%] of the subprocess $\gamma\gamma\to\rho^0\rho^0$, $\to\rho^0\pi^+\pi^-$, and $\to\pi^+\pi^-\pi^+\pi^-$ (NR) derived from a 3-parameter fit as a function of the four-momentum transfer squared $Q^2$

| $Q^2$ [GeV$^2$] | $\rho^0\rho^0$ | $\rho^0\pi^+\pi^-$ | $\pi^+\pi^-\pi^+\pi^-$ | $\chi^2$/NDF | NDF |
|---|---|---|---|---|---|
| 0.0–0.1 $\langle Q^2\rangle=0.008$ ($1.2\leqq W_{\gamma\gamma}\leqq 2.0$ GeV) | 65± 2 | 10± 6 | 25± 2 | see Table 1a | |
| 0.1–0.35 $\langle Q^2\rangle=0.28$ | 60±11 | 20±14 | 20± 9 | 1.2 | 28 |
| 0.35–0.55 $\langle Q^2\rangle=0.44$ | 43±10 | 29±15 | 28±11 | 1.1 | 29 |
| 0.55–1.0 $\langle Q^2\rangle=0.72$ | 23±14 | 50±18 | 27±12 | 1.2 | 19 |
| 2.0–16.0 $\langle Q^2\rangle=5.18$ | 26±18 | 32±25 | 42±17 | 0.5 | 8 |

**Table 4a.** Cross sections for the process $\gamma\gamma \to \pi^+\pi^-\pi^+\pi^-$ and the subprocess $\gamma\gamma \to \rho^0\rho^0$ from single-tag data as derived from a 2 parameter fit in the range $1.0\,\text{GeV} \leqq W_{\gamma\gamma} \leqq 1.9\,\text{GeV}$ and a 3-parameter fit for $W_{\gamma\gamma} \geqq 1.9\,\text{GeV}$ as a function of $W_{\gamma\gamma}$

| $W_{\gamma\gamma}$ [GeV] | $\sigma_{\pi^+\pi^-\pi^+\pi^-}$ [nb] (phase space acceptance corrected) | $\sigma_{\rho^0\rho^0}$ [nb] |
|---|---|---|
| 1.0–1.3 | $11 \pm 3$ | $2 \pm 2$ |
| 1.3–1.5 | $19 \pm 4$ | $9 \pm 4$ |
| 1.5–1.7 | $39 \pm 7$ | $29 \pm 7$ |
| 1.7–1.9 | $25 \pm 5$ | $18 \pm 5$ |
| 1.9–2.3 | $23 \pm 4$ | $6 \pm 4$ |
| 2.3–2.7 | $9 \pm 2$ | $4 \pm 2$ |
| 2.7–3.1 | $12 \pm 3$ | $3 \pm 2$ |

**Table 4b.** Cross sections for the process $\gamma\gamma \to \pi^+\pi^-\pi^+\pi^-$ and the subprocess $\gamma\gamma \to \rho^0\rho^0$ derived from a 3-parameter fit as a function of $Q^2$ averaged over $W_{\gamma\gamma}$ in the range $1.0 \leqq W_{\gamma\gamma} \leqq 3.1\,\text{GeV}$

| $Q^2$ [GeV$^2$] | $\sigma_{\pi^+\pi^-\pi^+\pi^-}$ [nb] (phase space acceptance corrected) | $\sigma_{\rho^0\rho^0}$ [nb] |
|---|---|---|
| 0.0–0.1 $\langle Q^2\rangle = 0.008$ | $85 \pm 3$ | $47 \pm 2$ |
| 0.1–0.35 $\langle Q^2\rangle = 0.28$ | $37 \pm 6$ | $22 \pm 5$ |
| 0.35–0.55 $\langle Q^2\rangle = 0.44$ | $25 \pm 4$ | $11 \pm 3$ |
| 0.55–1.0 $\langle Q^2\rangle = 0.72$ | $15 \pm 3$ | $4 \pm 2$ |
| 2.0–16.0 $\langle Q^2\rangle = 5.18$ | $5 \pm 1$ | $1 \pm 1$ |

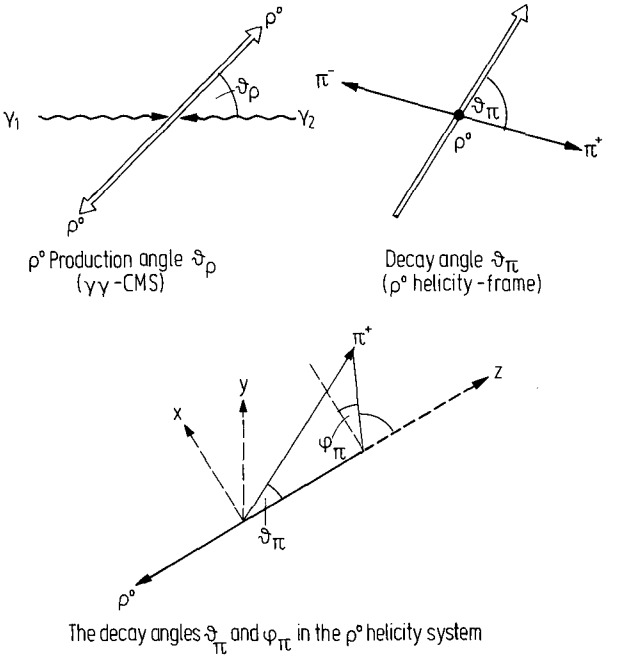


**Fig. 8.** Definition of the angular variables $\vartheta_\rho$, $\vartheta_\pi$, and $\varphi_\pi$

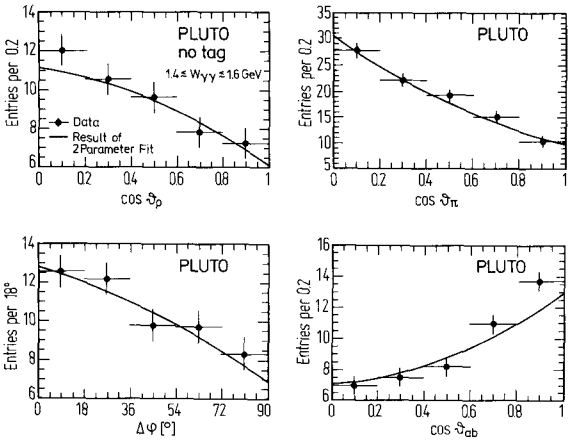


**Fig. 9.** Measured distributions of the angular variables $\vartheta_\rho$, $\vartheta_\pi$, $\vartheta_{ab}$ and $\Delta\varphi$. The full lines are angular distributions derived from incoherent sums of the model weighted isotropic four pion phase space Monte Carlo simulations

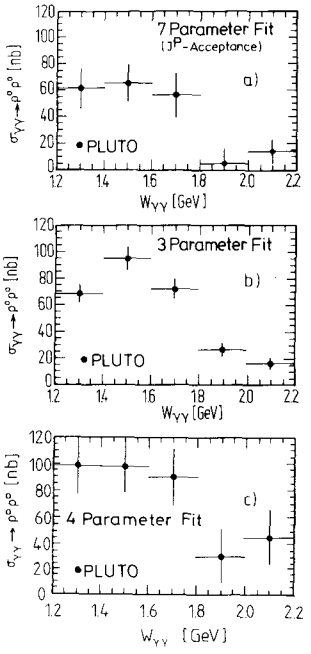


**Fig. 10a–c.** Cross sections for $\gamma\gamma \to \rho^0\rho^0$ derived from: **a** a 7-parameter fit including the proper $J^P$ acceptances, **b** a three parameter fit using isotropic production and decay, **c** a four parameter fit under the assumption that the $\rho^0\rho^0$-subprocess proceeds entirely via $J^P = 2^+$

### *3.5 Systematic errors*

The errors shown in the figures and tables in Sect. 3 are purely statistical. In addition, there are two further sources of uncertainty: The first is the systematic error estimated by assuming the detector acceptance to be known, with the following contributions:

**Table 5.** Fractions [%] of $J^P$ amplitudes contributing to the process $\gamma\gamma \to \rho^0\rho^0$

| $W_{\gamma\gamma}$ [GeV] Fractions [%] of Model | 1.2–1.4 | 1.4–1.6 | 1.6–1.8 | 1.8–2.0 | 2.0–2.2 |
|---|---|---|---|---|---|
| $0^+$ | 19±4 | 7±2 | 2±3 | −1±2 | 5±2 |
| $2^+(0)$ | 22±4 | 17±3 | 20±3 | 2±3 | 1±2 |
| $2^+(2)$ | 33±5 | 32±3 | 27±3 | 11±3 | 9±3 |
| $0^-$ | 6±3 | 5±2 | −3±2 | 4±2 | 0±2 |
| $2^-$ | −5±3 | 2±2 | −6±3 | −12±3 | 6±3 |
| $\rho^0\pi^+\pi^-$ | 21±4 | 20±4 | 38±5 | 59±5 | 53±5 |
| $\pi^+\pi^-\pi^+\pi^-$ (NR) | 4±3 | 17±3 | 22±3 | 37±3 | 26±4 |
| $\chi^2$/NDF (NDF = 39) | 2.1 | 2.1 | 1.4 | 0.8 | 0.5 |

**Table 6.** Cross sections (nb) for subprocess $\gamma\gamma \to \rho^0\rho^0$ corresponding to the different $J^P$ amplitudes and their sum. Also listed is the result of the 3-parameter fit (see Sect. 3.3)

| $W_{\gamma\gamma}$ (GeV) | $0^+$ | $2^+(0)$ | $2^+(2)$ | $0^-$ | $2^-$ | $\Sigma J^P$ | 3-parameter phase space |
|---|---|---|---|---|---|---|---|
| 1.2–1.4 | 12±3 | 26±5 | 23±4 | 5±2 | − 4±2 | 62±7 | 68±7 |
| 1.4–1.6 | 7±3 | 22±4 | 30±4 | 5±2 | 2±2 | 66±7 | 95±8 |
| 1.6–1.8 | 2±3 | 32±6 | 30±5 | −2±2 | − 5±2 | 57±9 | 73±8 |
| 1.8–2.0 | 0±1 | 2±4 | 10±3 | 3±2 | −10±2 | 5±6 | 27±5 |
| 2.0–2.2 | 3±2 | 1±2 | 8±3 | 0±2 | 3±1 | 15±4 | 17±4 |

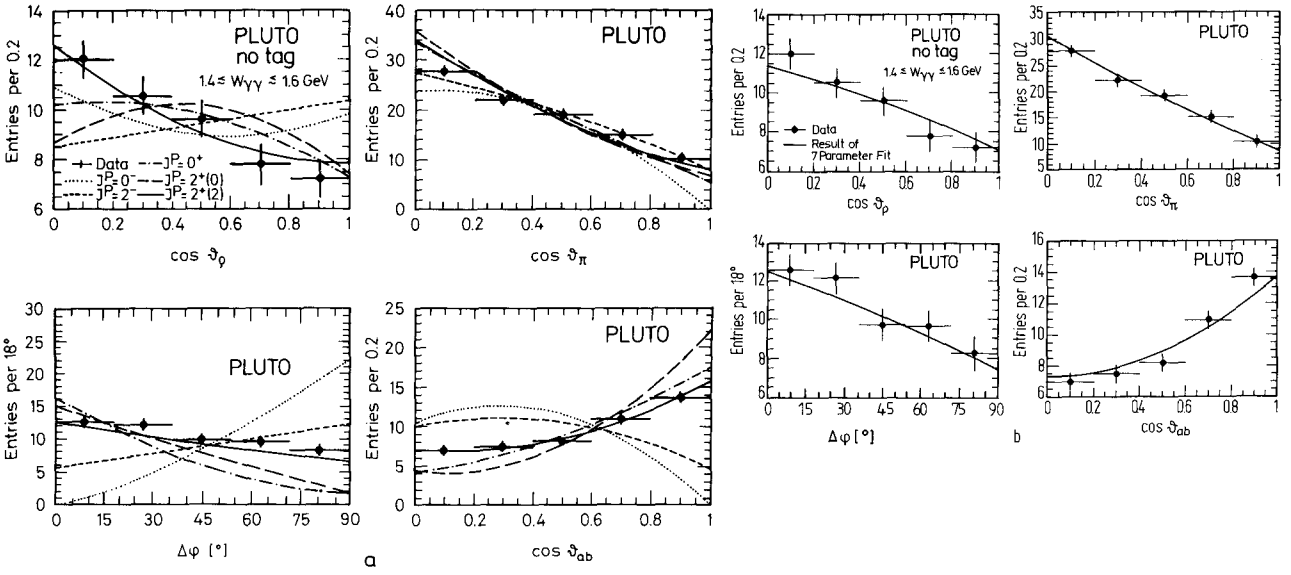


**Fig. 11. a** Angular distributions for five spin-parity assignments in comparison to the data. **b** Experimental angular distributions along with the results of a seven parameter fit ($\pi^+\pi^-\pi^+\pi^-$ (NR); $\rho^0\pi^+\pi^-$, five $J^P$ contributions to $\rho^0\rho^0$)

1) Uncertainty in the luminosity measurement [32] 3%
2) Monte Carlo integration of the photon spectra [27, 28] 5%
3) Uncertainty in the trigger simulation 4%
4) Contribution from background processes 4%
5) Uncertainty in the event selection 7%
6) Uncertainty in the determination of the pion absorption in the beam pipe and detector material [31] 6%
7) Background from incompletely measured events 3%

In total, this part of the systematic error is estimated to be 13%.

The dominant source of uncertainty in the cross

sections and fractions, however, comes from the necessity to use a specific model to calculate the acceptance corrections. The acceptances for different $J^P$ states and isotropic $\rho^0\rho^0$ phase space production differ considerably (see Fig. 4a, b). Also, the three fit procedures yield different $\rho^0\rho^0$ fractions. An estimate of this uncertainty can best be made from a comparison of the cross sections derived under different model assumptions (see Fig. 10). Realistically one must then attribute an error of $\approx 25\%$ to the cross sections. When comparing cross sections from different experiments special care must be taken to ensure that the same theoretical assumptions have been used to correct the measured data for detector acceptance.

## 4 Comparison and discussion

### *4.1 Comparison with other experiments*

Our no-tag cross section $\gamma\gamma \to \pi^+\pi^-\pi^+\pi^-$ is compared in Fig. 12 with the available data from Mark II, CELLO, and TPC/2$\gamma$ [3–5, 33, 34]. There is reasonable agreement for the entire range of $W_{\gamma\gamma}$. The same is true for the process $\gamma\gamma \to \rho^0\rho^0$ as presented in Fig. 13 in comparison to the data from other experiments (TASSO, CELLO, TPC/2$\gamma$ [2, 4–6, 33, 34]). Upper limits on the process $\gamma\gamma \to \rho^+\rho^-$ from JADE [7] are also shown. These are derived from exclusive $\pi^+\pi^0\pi^-\pi^0$ final states by requiring that the $\pi^\pm\pi^0$ mass combinations fall into a $\rho^\pm$ mass band.

Although the overall agreement of the PLUTO cross sections with the results of other experiments is satisfactory there is a tendency for the data points to be low in comparison to TASSO and TPC/2$\gamma$. This might be related to the fact that we have rejected in our analysis events with additional photons ($E_\gamma \geqq 100$ MeV) to obtain exclusive four pion events with minimal background.

Single-tag data are available from the TPC/2$\gamma$ Collaboration [5, 6, 33, 34] and TASSO [35]. Figure 14a shows a comparison of the $W_{\gamma\gamma}$ dependence of

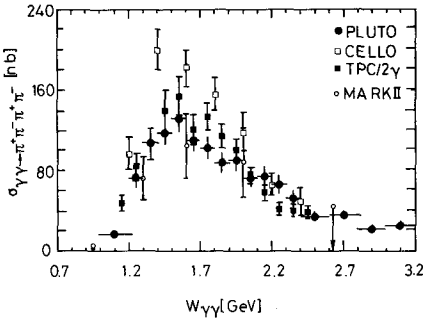


**Fig. 12.** Comparison of cross sections on the $\gamma\gamma \to \pi^+\pi^-\pi^+\pi^-$ no-tag data

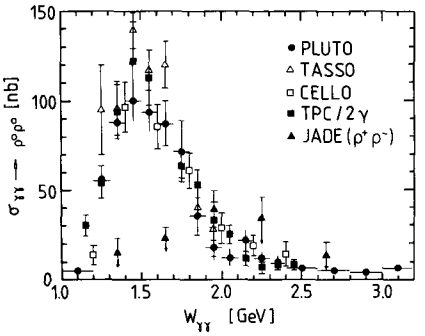


**Fig. 13.** Comparison of cross sections on the $\gamma\gamma \to \rho^0\rho^0$ no-tag data. Also shown are the upper limits of $\gamma\gamma \to \rho^+\rho^-$ from JADE [7]

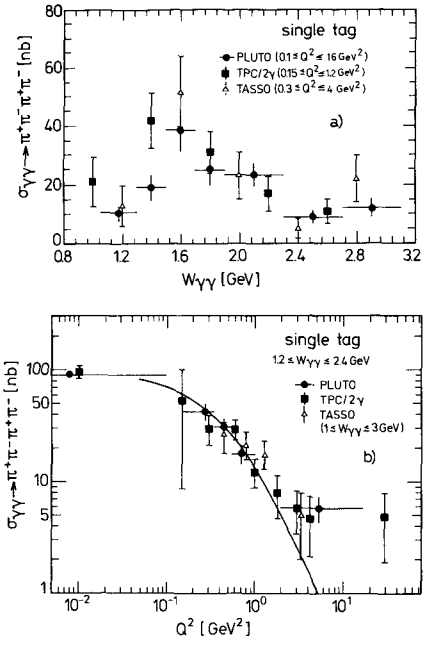


**Fig. 14. a** Comparison of single-tag cross sections for $\gamma\gamma \to \pi^+\pi^-\pi^+\pi^-$ as a function of $W_{\gamma\gamma}$. **b** Comparison of single-tag cross section for $\gamma\gamma \to \pi^+\pi^-\pi^+\pi^-$ as a function of $Q^2$. The solid line represents the VDM prediction

the single-tag cross section $\gamma\gamma \to \pi^+\pi^-\pi^+\pi^-$. The ranges of $Q^2$ for the different experiments are comparable since most of the data come from low $Q^2$. It can be seen in Table 2c that for low $Q^2$ $\rho^0\rho^0$ production still constitutes the dominant subchannel of the total cross section.

We have also determined the $Q^2$-dependence of the single-tag cross section in the $W_{\gamma\gamma}$ range $1.2\,\text{GeV} \leqq W_{\gamma\gamma} \leqq 2.4\,\text{GeV}$, to allow a direct comparison with the TPC/2$\gamma$ data (Fig. 14b). Also shown are the TASSO results [35] for the slightly different $W_{\gamma\gamma}$ range $1\,\text{GeV} \leqq W_{\gamma\gamma} \leqq 3\,\text{GeV}$. The $\rho$-pole prediction, normalized to the no-tag result (at $\langle Q^2 \rangle = 0.008\,\text{GeV}^2$), describes all three data sets well with the possible exception of the $Q^2$-range beyond $5\,\text{GeV}^2$

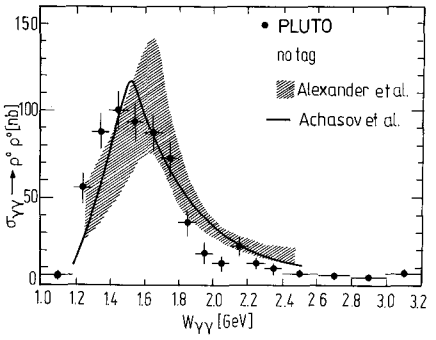


**Fig. 15.** Comparison of the no-tag cross section for $\gamma\gamma \to \rho^0\rho^0$ with predictions based on a four-quark model for an intermediate state decaying into $\rho^0\rho^0$ [13] and the results of a calculation based on factorization [8, 9]

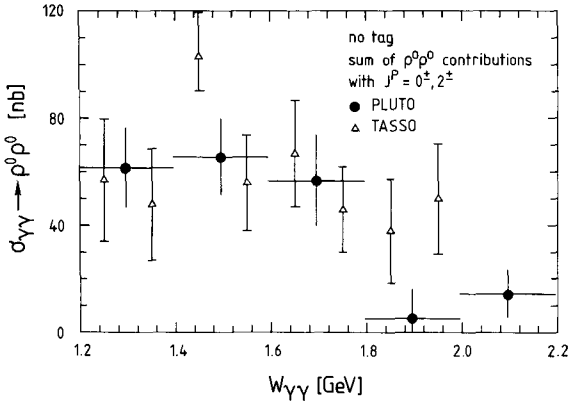


**Fig. 16.** Comparison of no-tag cross section for $\gamma\gamma \to \rho^0\rho^0$ using acceptance corrections from a fit with seven (PLUTO, see text) and six parameter (TASSO, [2])

where an excess is observed. This deviation appears to be more pronounced for the higher $W_{\gamma\gamma}$ ranges [5, 31].

The decomposition of the subprocess $\gamma\gamma \to \rho^0\rho^0$ into different partial waves excludes negative helicity states $(0^-, 2^-)$ and favours $J^P = 2^+$ over the wide range $1.2\,\text{GeV} < W_{\gamma\gamma} < 1.8\,\text{GeV}$ where the cross section is high. However $J^P = 0^+$ cannot be excluded for $W_{\gamma\gamma} < 1.4\,\text{GeV}$. These findings are in agreement with other experiments [4, 5]. TASSO [2] also finds $2^+$ dominance above 1.7 GeV, but a sizeable $0^+$ contribution below. The $\rho^0\rho^0$ cross section derived from our decomposition (Fig. 16) agrees with that of TASSO [2].

### *4.2 Comparison with models*

In the framework of vector meson dominance $\gamma\gamma$-scattering naturally leads to an enhanced $\rho^0\rho^0$-production since the photon couples directly to neutral but not to charged $\rho$'s. In this picture both photons are transformed into $\rho^0$'s which scatter off one another to give a final $\rho^0\rho^0$ state. In fact, one particular VDM approach [36] gives a cross section enhancement of the correct magnitude which, however, peaks at higher masses $W_{\gamma\gamma}$ than observed. Factorization approaches [8, 9] understand the large $\rho^0\rho^0$ cross section as a normal threshold behaviour as also observed in other resonance-free reactions, e.g. $K^+p \to K^+p, K^{*+}p$. They describe our measured cross section reasonably well (Fig. 15), and also the $Q^2$ dependence shown in Fig. 7.

Resonance based theories have to account for the large $\rho^0\rho^0$-production cross section and the absence of a comparable signal in $\gamma\gamma \to \rho^+\rho^-$ [7] (Fig. 13). The large difference excludes a $q\bar{q}$ resonance [10, 37]. In fact, the experimental upper limits [7] are compatible with a pure perturbative QCD description of $\rho^+\rho^-$-production [12]. Only four-quark models appear to be able to account for the difference between the $\rho^0\rho^0$ and $\rho^+\rho^-$ production [11, 13].

Our observed dominance of the $J^P = 2^+$ spin-parity state of the $\rho^0\rho^0$-system agrees with the four-quark model prediction [11, 13]. It does not contradict the phase space description, however, since the measured angular distributions can be reproduced in both.

Measurements of the photon-photon production of other vector mesons can in principle help to distinguish between the proposed explanations, because their predictions differ substantially in the processes $\gamma\gamma \to \rho^0\omega, \omega\omega, \phi\phi$ and $\rho^0\phi$. Previous upper limits on these processes [5, 6, 38, 39] were not sensitive enough to distinguish between different approaches. Recently, however, ARGUS [40, 41, 42, 43] has published cross sections for $\gamma\gamma \to \rho^0\omega$, $\gamma\gamma \to \omega\omega$, and $\gamma\gamma \to K^{*0}\overline{K^{*0}}$, and the TPC/Two-Gamma Collaboration has reported preliminary results on $\gamma\gamma \to \rho^0\omega$ [44]. Only part of their measured $\rho^0\omega$ production can be explained by the four-quark [13] and the $t$-channel factorization model [8, 9]. The observed strong enhancement of the $\omega\omega$ production cross section around 1.9 GeV, if confirmed, is hard to reconcile with any of the published explanations. The cross section for $\gamma\gamma \to K^{*0}\overline{K^{*0}}$ was found to be much larger than predicted by both the four-quark models [11, 13] and a QCD approach [12]. The upper limit by the ARGUS Collaboration on $\gamma\gamma \to \rho^0\phi$ [43] is considerably lower than the four-quark prediction, but agrees with the estimates from $t$-channel factorization [8, 9].

## 5 Summary

We have measured the four charged pion final states in $\gamma\gamma$-production under no-tag and single-tag condi-

tions in the kinematic range $1.0\,\text{GeV} \leqq W_{\gamma\gamma} \leqq 3.2\,\text{GeV}$ and $0\,\text{GeV}^2 \leqq Q^2 \leqq 16\,\text{GeV}^2$. The data show contributions from the phase space subprocesses $\rho^0\rho^0$, $\rho^0\pi^+\pi^-$, and $\pi^+\pi^-\pi^+\pi^-$ (NR) with a strong $\rho^0\rho^0$ component ($\sim 70\%$) for $1.2\,\text{GeV} \leqq W_{\gamma\gamma} \leqq 1.7\,\text{GeV}$. The incoherent superposition of these three subprocesses describes the observed angular distributions. A spin-parity analysis of the $\rho^0\rho^0$ system favours the $J^P = 2^+$ assignment, although $0^+$ cannot be excluded at low $W_{\gamma\gamma}$. Negative parity states $0^-$, $2^-$ are excluded. This analysis provides a constraint on resonance based models. The $\rho^0\rho^0$ cross section cannot be described by simple vector meson dominance models [14, 15], but is consistent with factorization estimates [8, 9] and with four-quark models [11, 13]. The $Q^2$-dependence of the cross section can adequately be described by a $\rho$-pole form factor and by factorization.

*Acknowledgements.* We gratefully acknowledge clarifying discussions with H. Kolanoski and U. Maor. We wish to thank the DESY directorate for the generous hospitality to the University groups, and are indebted to the PETRA machine group and the DESY computer center for their excellent performance during the experiment. We gratefully acknowledge the help of the technical groups in the design, construction, and maintenance of the apparataus. One of us (H.M./Siegen) wants to thank DESY and the University of Siegen for granting him a Ph.D. fellowship.

## References

1. TASSO Collab. R. Brandelik et al.: Phys. Lett. 97B (1980) 448
2. TASSO Collab. M. Althoff et al.: Z. Phys. C – Particles and Fields 16 (1982) 13
3. D.L. Burke et al.: Phys. Lett. 103B (1981) 153
4. CELLO Collab. H.J. Behrend et al.: Z. Phys. C – Particles and Fields 21 (1984) 205
5. TPC/Two-Gamma-Collab. A. Buijs et al.: contributed paper to the 23 Int. Conf. on High Energy Physics, Berkeley (1986)
6. A. Buijs: Ph. D. Thesis, Utrecht University (1986)
7. JADE Collab. J.E. Olsson: Proc. of the 5 Int. Colloquium on $\gamma\gamma$-Interactions, Aachen, p. 45; Ch. Berger (ed.), Lecture Notes in Physics, Vol. 191, Berlin, Heidelberg, New York: Springer (1983)
8. G. Alexander, U. Maor, P.G. Williams: Phys. Rev. D26 (1982) 1198
9. G. Alexander, A. Levy, U. Maor: Z. Phys. C – Particles and Fields 30 (1986) 65
10. K. Biswal, S.P. Misra: Phys. Rev. D26, (1982) 3020
11. Bing An Li, K.F. Liu: Phys. Lett. 118B (1982) 435, Erratum Phys. Lett. 124B (1983) 550; Phys. Rev. Lett. 51 (1983) 1510; Phys. Rev. D30 (1984) 613
12. S.J. Brodsky, G. Köpp, P.M. Zerwas: Phys. Rev. Lett. 58 (1987) 443
13. N.N. Achasov, S.A. Devyanin, G.N. Shestakov: Phys. Lett. 108B (1982) 134; Z. Phys. C – Particles and Fields 16 (1982) 55; Z. Phys. C – Particles and Fields 27 (1985) 99
14. M. Poppe: Int. J. Mod. Phys. A1 (1986) 545
15. H. Kolanoski: Two-photon physics at $e^+e^-$ storage rings. Springer Tracts in Modern Physics, Vol. 105, Berlin Heidelberg New York: Springer 1984
16. F. Erné: Proc. of the VI. Intern. Workshop on Photon-Photon Collisions, Lake Tahoe (1984)
17. J.H. Field: Photon-Photon Collisions. LPHNE (Univ. Paris VI and VII) Report 1984
18. M.T. Ronan: VII. Int. Workshop on Photon-Photon Collisions, Paris, 1986; Int. Rep. Lawrence Berkeley Lab. LBL-21817 (1986)
19. Ch. Berger, W. Wagner: Phys. Rep. 146 (1987) 2
20. L. Criegee, G. Knies: Phys. Rep. 83 (1982) 151
21. PLUTO Collab. Ch. Berger et al.: Z. Phys. C – Particles and Fields 26 (1984) 199
22. PLUTO Collab. Ch. Berger et al.: Z. Phys. C – Particles and Fields 33 (1987) 353
23. A.J. Tylka: DESY Internal Report, PLUTO 85-04 (1985)
24. TASSO Collab. M. Althoff et al.: Z. Phys. C – Particles and Fields 32 (1986) 11
25. Particle Data Booklet: Phys. Lett. 170B (1986) 1
26. S. Kawabata: Program Writeup (1982, unpublsihed); Comp. Phys. Commun. 41, (1986) 127; Contribution to the parallel session, reported by J.H. Field: Proc. of the IV International Symposium on Photon-Photon Interactions, Paris 1981, p. 447. See also G.P. Lepage: J. Comp. Phys. Commun. 27 (1978) 192; VEGAS – Adaptive Multi-dimensional Integration Program. CLNS – 80/447 (1980)
27. V.M. Budnev et al.: Phys. Rep. 15 (1975) 181
28. M. Feindt: Internal Report. DESY-PLUTO 84-03 (1984)
29. J.D. Jackson: Nuovo Cimento 34 (1964) 1644
30. J.J. Sakurai, D. Schildknecht: Phys. Lett. 40B (1972) 121
31. H. Müller: Ph. D. Thesis Siegen University (1987)
32. H. Kapitza: Internal Report, DESY-PLUTO 85-05 (1985)
33. PEP4/PEP9 Collaboration, XXII. Int. Conf. on High Energy Physics, contributed paper, Leipzig (1984)
34. W. Ko: XXII. Int. Conf. on High Energy Physics, Leipzig, Vol. 1, (1968) p. 335
35. T. Kracht: Ph. D. Thesis, Hamburg Univ. 1987
36. M. Hatzis, J. Paschalis: Lett. Nuovo Cimento Vol. 40 (1984) 362
37. M. Krammer: private communication, see [15]
38. PLUTO Collab. Ch. Berger et al.: Z. Phys. C – Particles and Fields 29 (1985) 183
39. JADE Collab. Europhysics Conf. on High Energy Physics, Brighton (1983), presented by J.B. Dainton, p. 652
40. ARGUS Collab. A. Nilsson: VII. Int. Workshop on Photon-Photon Collisions, Paris, France, (1986)
41. ARGUS Collaboration, H. Albrecht et al.: Phys. Lett. B196 (1987) 101
42. ARGUS Collab. H. Albrecht et al.: Phys. Lett. B198 (1987) 577
43. ARGUS Collab. H. Albrecht et al.: Phys. Lett. B198 (1987) 255
44. TPC/Two-Gamma Collab. H. Aihara et al.: Contributed paper to the 1987 International Symposium on Lepton and Photon Interactions at High Energies, Hamburg, 1987